3

Faraday Isolators for High Average Power Lasers

Efim Khazanov
Institute of Applied Physics of the Russian Academy of Science, N. Novgorod
Russia

1. Introduction

The average power of solid-state and fiber lasers has considerably increased during the last ten years. The 10 kW power is not record-breaking any longer, and a topical problem nowadays is to create lasers with a power of 100 kW. Therefore, the study of thermal effects caused by absorption of laser radiation in the bulk of optical elements becomes ever more important. The Faraday isolator (FI) strongly depends on these effects because its magneto-optical elements (MOEs) are relatively long and its absorption α_0 is 10^{-3}…10^{-2} cm^{-1}, see Table 1. As a result, heat release power is at least tenths of percent of transmitted laser power P_0.

	V 1.06 μm	$\frac{1}{V}\frac{dV}{d\Gamma}$	κ	α_0	ξ	α_T	$\|Q\|$	dn/dT	P
	rad/T/m	10^{-3}/K	W/K/m	10^{-3}/cm		10^{-7}/K	10^{-7}/K	10^{-6}/K	10^{-6}/K
TGG	39 [1; 2] 35 [3-5] 36 [6] 40 [7]	3.5 [8]	4.4±0.1 [9] 4.5±0.5 [10] 5.3±0.5 [11] 7.4 [5; 12-15]	2 [15] 1-6 [14] 4.8 [13] 1.4-4.2 [16] 2.5 [17] 1.6 [18]	2.2 [16] 2.25 [13]	94 [15] 67-72 [9] 40[5]	17 [13] *)	20 [15] 19 [13] 18-21 [9]	17 [13] *)
MOC101	8.7 [1; 2; 19]	4 [19]		1 [1]; 2.3 [19]	1				
MOC105	17 [1]; 18 [2; 19]	5 [19]	0.51 [20]	2.3 [19]	1	82 [21]	6 [20]	0.6 [21]	
MOC04	21 [1; 2; 19]		0.74 [20]	1 [1]; 2.3 [19]	1	49 [21]	9 [20]	8.7 [21]	
MOC10	28 [2; 19]; 26 [1]		0.68 [20]	2 [1]; 4.6 [19]	1	56 [21]	8.5 [20]	8.5 [21]	
FR–5	21 [1; 4]	3.4 [22]	0.84 [15]	3 [1]; 10 [15]	1	47 [15]	9 [20]	7.5 [15]	

Table 1. Property of magneto-optical materials. MOC 10 is analog of M-24 (Kigre, USA).

*) assuming κ=5W/Km;

[1](Zarubina & Petrovsky, 1992), [2](Zarubina et al., 1997), [3](Chen et al., 1998), [4](Jiang et al., 1992), [5](Kaminskii et al., 2005), [6](Yasuhara et al., 2007), [7](Raja et al., 1995), [8](Barnes & Petway, 1992), [9](Ivanov et al., 2009), [10](Slack & Oliver, 1971), [11](Chen et al., 1999), [12](Wynands et al., 1992), [13](Khazanov et al., 2004), [14](Mueller et al., 2002), [15](Mansell et al., 2001), [16](Khazanov et al., 2002a), [17](Mukhin et al., 2009), [18](VIRGO-Collaboration, 2008), [19](Malshakov et al., 1997), [20](Andreev et al., 2000a), [21](Zarubina, 2000), [22](Davis & Bunch, 1984).

Source: Advances in Solid-State Lasers: Development and Applications, Book edited by: Mikhail Grishin,
ISBN 978-953-7619-80-0, pp. 630, February 2010, INTECH, Croatia, downloaded from SCIYO.COM

At P_0=100 W (and higher) this gives rise to polarization distortions deteriorating the isolation degree, and phase distortions – aberrations. Many applications require a combination of high average power, high isolation degree, and small aberrations. Below we shall demonstrate that although the methods well known for laser amplifiers can be used for analyzing thermal effects in FI, yet one has to take into account specific features imposed by the magnetic field (the Faraday effect). We shall overview theoretical and experimental results of investigations of thermal effects in FIs and methods for their compensation and suppression. Note that all the results reported below are valid not only for cw lasers but for pulse lasers with high repetition rate as well.

Unlike FI, a Faraday mirror proposed in (Giuliani & Ristori, 1980) is used not for optical isolation, but for compensation of birefringence in laser amplifiers (Carr & Hanna, 1985), oscillators (Giuliani & Ristori, 1980), regenerative amplifiers (Denman & Libby, 1999) and fiber optics as well (Gelikonov et al., 1987). Despite the great similarity between the Faraday mirror and FI, there are two primary differences between them. First, the isolation in FI is governed only by the depolarization in the second pass, whereas in the Faraday mirror the polarization distortions are accumulated during both the passes. Second, the radiation that is incident on the MOE in FI is linearly polarized, whereas the radiation that is incident on the Faraday mirror has already been depolarized. We shall consider only FI; a Faraday mirror for high power lasers is studied in (Khazanov, 2001; Khazanov et al., 2002b; Khazanov, 2004).

In the absence of thermal effects in the MOE after the first pass (from left to right), a beam retains its horizontal polarization (Fig. 1, 2) and passes through polarizer 4, while during the return pass (from right to left), the polarization is altered to vertical and the beam is reflected by polarizer 1.

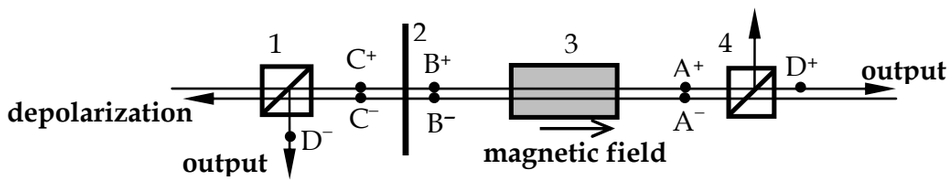

Fig. 1. Traditional design of a Faraday isolator. 1,4 – polarizers; 2 – λ/2 plate; 3 – MOE.

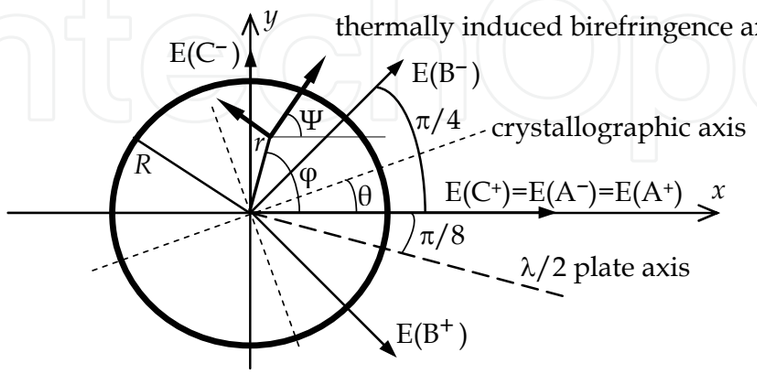

Fig. 2. Cross-section of magneto-optical crystal: *r, φ* are polar coordinates; θ is angle of inclination of the crystallographic axis; Ψ is angle of inclination of eigen polarization of thermally induced birefringence.

The light absorption in MOE generates a temperature distribution that is nonuniform over a transverse cross section. This leads to three physical mechanisms affecting the laser radiation: i) wave front distortions (thermal lens) caused by the temperature dependence of the refraction index; ii) nonuniform distribution of the angle of polarization rotation because of the temperature dependence of the Verdet constant and thermal expansion of the MOE; and iii) simultaneous appearance not only of the circular birefringence (Faraday effect), but also of the linear birefringence caused by mechanical strains due to the temperature gradient (photoelastic effect).

The first mechanism (Zarubina et al., 1997) does not induce any polarization changes in laser radiation and hence does not affect the isolation degree. The latter two mechanisms do alter the polarization state of radiation. The temperature dependence of the Verdet constant and thermal expansion lead to changes of the phase shift between eigen polarizations which remain circular (Wynands et al., 1992). The photoelastic effect not only changes the phase shift between eigen polarizations, but also alters the eigen polarizations themselves, which become elliptical (Khazanov, 1999; Khazanov et al., 1999). In section 2 we discuss the influence of all thermal effects on FI parameters and determine the figure of merit of magneto-optical materials for high average power lasers.

Thermal effects in FI may be compensated by some additional optical elements or suppressed (reduced) by choosing optimal FI parameters or geometries. Section 3 is devoted to compensation of thermal lens (by means of an ordinary negative lens or a negative thermal lens) and compensation of depolarization (by means of crystalline quartz placed inside a telescope or by means of replacing one 45^0 MOE by two 22.5^0 MOEs and a $\lambda/2$ plate or a 67.5^0 polarization rotator between them).

In section 4 we discuss the methods of thermal effects suppression: cooling FI to liquid nitrogen temperature, shortening MOE using a strong magnetic field, employing several thin discs cooled through optical surfaces, and using slabs and rectangular beams.

2. Thermal effects in Faraday isolators

2.1 Jones matrix of thermally loaded magneto-optical element

A non-uniformly heated MOE is a polarization phase plate that has simultaneously two types of birefringence: circular due to the Faraday effect, and linear due to the photoelastic effect. The circular birefringence is completely described by a phase shift between circular eigen polarizations δ_c; the polarization rotation angle is $\delta_c/2=VBL$, where B is magnetic field, V and L are Verdet constant and length of MOE. Linear birefringence is described by a phase shift between linear eigen polarizations δ_1 and an inclination angle Ψ of eigen polarization relative to the x axis (Fig. 2). Such a polarization phase plate is described by the Jones matrix (Tabor & Chen, 1969)

$$F(\delta_c,\delta_l,\Psi)=\exp(ikLn_0)\exp\left(ikL\left[T(r)-T(0)\right]P\right)\sin\frac{\delta}{2}\begin{pmatrix}\cot\frac{\delta}{2}-i\frac{\delta_l}{\delta}\cos 2\Psi & -\frac{\delta_c}{\delta}-i\frac{\delta_l}{\delta}\sin 2\Psi\\ \frac{\delta_c}{\delta}-i\frac{\delta_l}{\delta}\sin 2\Psi & \cot\frac{\delta}{2}+i\frac{\delta_l}{\delta}\cos 2\Psi\end{pmatrix}, \quad (1)$$

where

$$P=\frac{dn}{dT}-\alpha_T\frac{n_0^3}{4}\frac{1+\nu}{1-\nu}\cdot(p_{11}+p_{12}) \quad (2)$$

is a thermo-optical constant of MOE, $\delta^2 = \delta_l^2 + \delta_c^2$, and n_0, ν, α_T, $p_{i,j}$ are "cold" refractive index, Poisson's ratio, thermal expansion coefficient, and photoelastic coefficients, respectively, $k=2\pi/\lambda$, λ is wavelength in vacuum. Here and further we assume that the temperature T is uniform along the direction of beam propagation z. The second exponential factor in (1) has no influence upon polarization distortions and is an isotropic thermal lens. A contribution to this lens is made by the temperature dependence of the refraction index and "isotropic" part of the photoelastic effect (see two corresponding terms in (2)). We also assume that the contribution of thermal expansion is negligibly small in comparison with the temperature dependence of the refractive index; and magnetic field B (and hence δ_c) does not depend on the longitudinal coordinate z. The case when B depends on z was considered in (Khazanov et al., 1999).

For rod geometry δ_l and Ψ are defined by the formulas (Soms & Tarasov, 1979):

$$\delta_l = 4\pi \frac{L}{\lambda} Qq(\varphi) \left(\frac{1}{r^2} \int_0^r r^2 \frac{dT}{dr} dr \right) \tag{3}$$

$$\tan(2\Psi - 2\theta) = \xi \tan(2\varphi - 2\theta)\,, \tag{4}$$

where

$$q(\varphi) = \begin{cases} \sqrt{\cos^2(2\varphi - 2\theta) + \xi^2 \sin^2(2\varphi - 2\theta)} & for\ [001] \\ (1+2\xi)/3 & for\ [111] \end{cases} \tag{5}$$

$$Q = \left(\frac{1}{L} \frac{dL}{dT} \right) \frac{n_0^3}{4} \frac{1+\nu}{1-\nu} \cdot (p_{11} - p_{12}) \tag{6}$$

$$\xi = \frac{2p_{44}}{p_{11} - p_{12}}\,. \tag{7}$$

Parameter of optical anisotropy ξ shows the difference of the cubic crystal from glass (for all glasses ξ=1). It can be seen from (3-7) that expressions for δ_1 and Ψ for the [111] crystal orientation can be obtained from the corresponding expressions for the [001] orientation by making a formal substitution:

$$\xi \to 1, \quad Q \to Q(1+2\xi)/3 \quad \text{(for the transition [001] } \to \text{ [111])}. \tag{8}$$

Further we shall give all results only for the [001] orientation, having in mind that the corresponding formulas for the [111] orientation can be obtained by substituting (8). Arbitrary crystal orientation is analyzed in (Khazanov et al., 2002a).

For the Gaussian beam with radius r_0 and power P_0 one may substitute the solution of the heat conduction equation

$$\frac{dT}{dr} = -\frac{\alpha P_0}{2\pi\kappa} \cdot \frac{1 - \exp(-r^2 / r_0^2)}{r} \tag{9}$$

into (3):

$$\delta_l(u,\varphi) = p\frac{u+\exp(-u)-1}{u}\sqrt{\cos^2(2\varphi-2\theta)+\xi^2\sin^2(2\varphi-2\theta)}\,, \tag{10}$$

where

$$p = \frac{L}{\lambda}\frac{\alpha_0 Q}{\kappa}P_0\,, \tag{11}$$

$u=r^2/r_0^2$, α_o and κ are absorption and thermal conductivity. Dimensionless parameter p physically means normalized laser power. Assuming for a TGG crystal L/λ=20000, $\alpha_0=1.5\cdot10^{-3}\text{cm}^{-1}$, $Q=17\cdot10^{-7}\text{K}^{-1}$, and κ=5W/Km we obtain p=1 when P_0=1kW.
Formula for δ_c follows from the Faraday effect, taking into account the temperature dependence of the Verdet constant and thermal expansion:

$$\delta_c(r) = \delta_{co}\left[1+\left(\frac{1}{V}\frac{dV}{dT}+\alpha_T\right)\left(-T(r)-T\left(r^*\right)\right)\right], \tag{12}$$

where δ_{co} is a doubled angle of polarization rotation at $r=r^*$; and r^* can be chosen such as to minimize depolarization, see below. Thus, Jones matrix of MOE is determined by (1) with (4, 10, 12).

2.2 Polarization distortions (depolarization)

Let us calculate the depolarization ratio of the beam after the second pass through the FI (Fig. 1). In the absence of thermal effects, the beam at a point C^- is vertically polarized and is reflected by polarizer 1. Because of the thermal effects there occurs depolarized radiation, which, being horizontally polarized at a point C^-, passes through polarizer 1. The local depolarization ratio $\Gamma(r,\varphi)$ is

$$\Gamma(r,\varphi) = \left|\boldsymbol{E_C}\boldsymbol{x}_0\right|^2 / \left|E_C\right|^2\,, \tag{13}$$

where $\boldsymbol{E}_C$ is the complex amplitude of the field at point C^-. Of major interest is the integral depolarization γ (the isolation degree of the FI is $1/\gamma$) that is a fraction of horizontally polarized radiation power at point C^-:

$$\gamma = \int_0^{2\pi} d\varphi \int_0^{\infty} \left|\mathbf{E}_C\mathbf{x}_0\right|^2 r dr \Bigg/ \int_0^{2\pi} d\varphi \int_0^{\infty} \left|E_C\right|^2 r dr = \frac{1}{\pi r_0^2}\int_0^{2\pi} d\varphi \int_0^{\infty} \Gamma \exp\left(\frac{-r^2}{r_0^2}\right) r dr\,. \tag{14}$$

Here we assume that the FI aperture is such that aperture losses can be neglected, i.e. the integration in (14) over a polar radius r can be extended to infinity; and the beam at a point A^- has Gaussian shape and horizontal polarization:

$$\mathbf{E}(A^-) = const\ \mathbf{x}_0 \exp\left(-r^2/2r_0^2\right). \tag{15}$$

Knowing Jones matrices of all elements, the field at points C^- can be easily found:

$$\mathbf{E}(C^{-}) = \mathbf{L}_2(3\pi/8)\mathbf{F}(\delta_c=\pi/2, \delta_l)\mathbf{E}(A^{-}), \tag{16}$$

where $\mathbf{L_2(\beta_L)}$ is the matrix of a $\lambda/2$ plate with an angle of inclination of the optical axis β_L:

$$\mathbf{L}_2(\beta_L) = \begin{pmatrix} \cos 2\beta_L & \sin 2\beta_L \\ \sin 2\beta_L & -\cos 2\beta_L \end{pmatrix}. \tag{17}$$

Substituting (1, 15, 17) into (16), and the result into (13, 14) yields Γ and γ. Let us consider the case when the linear birefringence is small

$$\delta_l << 1 \tag{18}$$

and changes of the polarization rotation angle are small too, i.e. $(\delta_c(r)-\delta_{co}) << \delta_{co}$. In this case from (13) accurate to within terms of order δ_l^4 and $\delta_l^2(\delta_c - \delta_{c0})$ we obtain

$$\Gamma = \frac{2\delta_l^2}{\pi^2}\sin^2\left(2\Psi - \frac{\pi}{4}\right) + \left(\frac{\delta_c}{2} - \frac{\pi}{4}\right)^2. \tag{19}$$

The substitution of (4, 10, 12) into (19), and the subsequent substitution of the result into (14) yield

$$\gamma = p^2\frac{A_1}{\pi^2}\left(1 + (\xi^2 - 1)\cos^2\left(\frac{\pi}{4} - 2\theta\right)\right) + \left(\frac{\pi^2}{16}\right)\left(\frac{1}{V}\frac{dV}{dT} + \alpha_T\right)^2 \cdot \int_0^\infty \exp(-u)(T(r) - T(r^*))^2\, du, \tag{20}$$

where A_i are given in Table 2. By rotating the MOE around z axis, i.e. by varying angle θ, one can minimize the first term in (20). By differentiating (20) over r^* and equating the derivative to zero, we obtain for the optimal value $r_{opt} \approx 0.918 r_0$. In practice, when choosing the value of the magnetic field or length of the MOE, one should secure rotation of polarization by an angle $\pi/4$ at point $r=0.918r_0$, see (12). As a result of these two optimizations we obtain

$$\gamma_{\min} = \frac{A_1}{\pi^2}p^2 + A_3\left(\frac{\alpha_0 P_0}{16\kappa}\right)^2\left(\frac{1}{V}\frac{dV}{dT} + \alpha_T\right)^2. \tag{21}$$

Thus, depolarization (19, 20, 21) is an arithmetic sum of contributions of two effects: the photoelastic effect (the first term) and temperature dependence of Verdet constant (the second term). Note that both terms in (20, 21) are independent of the beam radius r_0 and are proportional to the square of laser power P_0. Expression (21) allows us to compare the impacts of these effects. Assuming $L/\lambda \cong 20000$ and taking into account data in Table 1 one can show that the photoelastic effect is dominating. This fact found numerous experimental evidences. The most illustrative one is the transverse distribution of $\Gamma(r, \varphi)$. If temperature dependence of the Verdet constant is neglected, $\Gamma(r,\varphi)$ according to (4, 19) has the form of a cross, and the axes of this cross (directions where $\Gamma=0$) are rotated relative to the x, y axes by an angle $\pi/8$. This completely conforms to the experimental data, see Fig. 3.

m	**1**	**2**	**8**	∞
$A_0(m)=\sigma_1/\sigma_0$	1	0.56	0.48	1/2
$A_1(m)=\frac{1}{\sigma_0^3}\cdot\int_0^\infty\frac{h_m^2(u)du}{\exp(u^m)}$	0.137	0.111	0.087	1/12
$A_2(m)=\frac{1}{\sigma_0^5}\cdot\int_0^\infty\frac{h_m^4(u)du}{\exp(u^m)}$	0.042	0.0265	0.0145	1/80
$A_3(m)=\frac{1}{\sigma_0^3}\cdot\int_0^\infty\frac{f_m^2(u)}{\exp(u^m)}du-\frac{1}{\sigma_0^4}\left[\int_0^\infty\frac{f_m(u)}{\exp(u^m)}du\right]^2$	0.268	0.158	0.092	1/12
$A_4(m)=A_3(m)-\frac{\sigma_1^2}{\sigma_0^4}\frac{1}{\sigma_2\sigma_0-\sigma_1^2}\left[\int_0^\infty\frac{f_m(u)}{\exp(u^m)}(1-\frac{u\sigma_0}{\sigma_1})du\right]^2$	0.0177	0.0021	10^{-5}	0
$A_5(m)=A_1(m)-\frac{1}{\sigma_2\sigma_0^3}\left(\int_0^\infty\frac{uh_m(u)}{\exp(u^m)}du\right)^2$	0.012	0.0017	10^{-5}	0
$A_6(m)=\frac{m^2}{\sigma_0}\int_0^\infty\frac{w_m^2(u)}{u^2\exp(u^m)}du$	0.046	0.054	0.028	0
$A_7(m)=\frac{m^4}{\sigma_0}\int_0^\infty\frac{w_m^4(u)}{u^4\exp(u^m)}du$	0.0031	0.0076	0.0082	0
$h_m=\frac{1}{u}\int_0^u dz\int_0^z\frac{dy}{\exp(y^m)}$ $\quad f_m=\int_0^u\left(\int_0^z\frac{dy}{\exp(y^m)}\right)\frac{dz}{z}$ $\quad w_m=\int_0^u\frac{z^m dz}{\exp(z^m)}$ $\quad \sigma_k(m)=\int_0^\infty\frac{y^k dy}{\exp(y^m)}$				

Table 2. Values $A_{0\text{-}7}$ for different m. $A_i \equiv A_i(m=1)$.

Fig. 3. Theoretical (a) and experimental (b) (Khazanov et al., 2000) intensity distributions of depolarized beam.

In addition, experiments on depolarization compensation (see sections 3.2, 3.3) also confirmed domination of the photoelastic effect. Further we shall assume that γ is given by

$$\gamma = A_1 p^2 / \pi^2 . \tag{22}$$

Thermal effects influence not only depolarization γ, but also power losses during the forward pass γ_1, i.e. losses caused by the reflection of depolarized radiation from polarizer 4 (Fig.1). Considering only the photoelastic effect, by analogy with γ an expression for γ_1 at $\theta=\theta_{opt}$ may be found (Khazanov, 2000):

$$\gamma_1 = A_1 \xi^2 p^2 / \pi^2 . \tag{23}$$

Deriving (23) we neglected average over cross-section decrease of V due to average heating of MOE (Khazanov et al., 1999). An increase of the laser power from 0 to 400 W decreased the angle of rotation by 2 degrees (Mukhin et al., 2009), which corresponded to a negligible in practice value $\gamma_1 \approx 0.1\%$. However, when FI is placed in vacuum, the average temperature (and hence γ_1) increases much higher (VIRGO-Collaboration, 2008). In this case good thermal contact of MOE with magnets housing and/or thermal stabilization of the MOE by the Peltier element should be implemented to keep γ_1 negligible.

2.3 Amplitude and phase distortions

The depolarization ratio γ and power losses during the first pass γ_1 are generally the main but not the only parameters of the FI. The output radiation $\mathbf{E}_{out}$ has also spatial (amplitude and phase) distortions. Depending on particular FI applications, the output beam may be a beam at point D^+, a beam at point D^-, or both (Fig. 1). Below we shall assume the first, most frequently used case. For quantitative description of the spatial distortions we shall use

$$\gamma_s = 1 - \left| \int_0^{2\pi} d\varphi \int_0^{\infty} E_{out} E_{ref}^* r dr \right|^2 \Bigg/ \left(\int_0^{2\pi} d\varphi \int_0^{\infty} \left| E_{out} \right|^2 r dr \cdot \int_0^{2\pi} d\varphi \int_0^{\infty} \left| E_{ref} \right|^2 r dr \right), \tag{24}$$

i.e. the difference from unity of the overlapping integral of E_{out} and the reference field E_{ref} that is the field in the absence of thermal effects. To determine analytical expressions for γ_s we shall apply the formalism of the Jones polarization matrices as above. In case of weak polarization distortions (18) and weak phase distortions, i.e. $kL(n(r)-n(0))<<1$, we obtain

$$\gamma_s = \gamma_a + \gamma_i , \tag{25}$$

where

$$\gamma_a = p^2 A_1 / \pi^2 \qquad \gamma_i = p_i^2 A_3 / 4 \tag{26}$$

$$p_i = \frac{L}{\lambda} \frac{\alpha_0 P}{\kappa} P_0 . \tag{27}$$

Values of all γ are summarized in Table 3. Let us discuss the results obtained. First of all, it is important to note that γ_s (as well as γ and γ_1) does not depend on r_0 and is proportional to the square of P_0. Two physical effects contribute to γ_s: isotropic thermal lens (γ_i) and anisotropic distortions (γ_a) due to depolarization. The latter contribution is attributed to the distortions non-uniformity over the cross-section resulting in appearance of amplitude and phase distortions in the beam after propagation through the polarizer (e.g., Maltese cross, astigmatism). Taking into account polarization losses at the first pass γ_1, the total power loss in spatial and polarization mode after the first pass through the FI is $\gamma_{total}=\gamma_1+\gamma_a+\gamma_i$.

		Traditional FI Fig. 1	FI with $\lambda/2$ Fig. 9a	FI with 67.5^0 rotator Fig. 9b
depolarization ratio γ (isolation degree is $1/\gamma$)		$p^2 A_1 / \pi^2$	$p^4 \frac{8A_2}{\pi^4} \xi^2 \left(b^2 - a^2\right)$ ξ>1.3	$p^4 \frac{6a^2 A_2}{\pi^4} \left(1 + \frac{2}{3}\xi^2 + \xi^4\right)$
no thermal lens compensation	polarization losses γ_1	$p^2 A_1 \xi^2 / \pi^2$	$\frac{p^2 A_1}{\pi^2}\left(2 - \frac{\pi}{2}\right)\left(\xi^2 + 1\right)$ ξ>1.3	$p^2 A_1 \left(2 - \sqrt{2}\right) / \pi^2$
	anisotropic losses γ_a	$p^2 A_1 / \pi^2$	$0(p^4)$	$p^2 A_1 \left(2 - \sqrt{2}\right) \xi^2 / \pi^2$
	isotropic losses γ_i	$p_i^2 A_3 / 4$	$p_i^2 A_3 / 4$	$p_i^2 A_3 / 4$
telescope compensation	γ_{1TC}	γ_1	γ_1	γ_1
	γ_{aTC}	γ_a	γ_a	γ_a
	γ_{iTC}	$p_i^2 A_4 / 4$	$p_i^2 A_4 / 4$	$p_i^2 A_4 / 4$
adaptive compensation	γ_{1AC}	$\gamma_1 + A_1 p_{CG}^2 / 8$	$\gamma_1 + A_1 p_{CG}^2 / 8$	$\gamma_1 + A_1 p_{CG}^2 / 8$
	γ_{aAC}	$\gamma_1 + \frac{A_1}{8} p_{CG}^2 + \frac{A_1 \xi}{\pi\sqrt{8}} p p_{CG}$		
	γ_{iAC}	0	0	0

Table 3. Depolarization and power losses after the first pass through FI.

Note that the parameter p_i (27) is analogous to the parameter p (11) accurate within replacement of thermo-optical constants: Q (6) characterizing anisotropic distortions by P (2) characterizing isotropic distortions. Isotropic losses γ_i are determined only by parameter p_i, while p determines isolation degree $1/\gamma$ as well as losses γ_a and γ_i induced by anisotropy of the photoelastic effect.

Since the temperature distribution is not parabolic the thermal lens is aberrational. Such a lens can be represented as a sum of a parabolic lens with focus F and an aberrator that does not introduce any geometrical divergence. Using the method of moments an expression for F can be obtained (Poteomkin & Khazanov, 2005):

$$F = \frac{2A_0}{p_i} k r_0^2, \tag{28}$$

where A_0 is given in Table 2.

2.4 The influence of beam shape

Above we have discussed thermal distortions of a Gaussian beam. Since a laser beam induces (being a heat source) and simultaneously reads distortions, the value of self-action may depend significantly on the transverse distribution of the intensity. The results obtained can be generalized for an arbitrary axially symmetric beam (Khazanov et al., 2002b), including a super-Gaussian beam with power P_0 and intensity

$$I(r) = P_0 \exp\left(-\frac{r^{2m}}{r_0^{2m}}\right) \cdot \left(\pi r_0^2 \int_0^\infty \exp(-y^m) dy\right)^{-1}. \tag{29}$$

At m=1 the beam is Gaussian, and at m=∞ the beam turns into a flat-top one. Repeating the procedure described in sections 2.2, 2.3 for the laser beam (29) instead of (15), one can show that expressions for the depolarization ratio γ (19-22), for losses in polarization γ_1 (23), and spatial γ_s (25-26) mode during the first pass, and for F (28) are valid at any m, if A_i are replaced by $A_i(m)$, expressions for which are given in Table 2. All equations below are for a Gaussian beam, but they are valid for a super-Gaussian beam after this replacement.
Note that with increasing m the value of $A_{1,3}(m)$ decreases. This means that a flat-top beam is optimal for decreasing the influence of all thermal effects, whereas a Gaussian beam has the strongest self-action.

2.5 Selection of magneto-optical medium

In high-power lasers, magneto-optical materials are chosen taking into account specific features of different nonlinear effects. As a result, figures of merit were introduced: the larger the figure of merit, the better the medium. From the point of view of power losses due to absorption, such a figure of merit is the V/α_0 ratio (Robinson, 1964). From the point of view of self-focusing in pulse lasers, this is parameter VW_{cr} (Zarubina et al., 1997) for thermal self-focusing and VP_{cr} (Malshakov et al., 1997) for electronic Kerr self-focusing.
As has been shown in sections 2.2 and 2.3, all thermal effects are determined by p_i and p. Taking into account that L~1/V we obtain figures of merit μ_i and μ:

$$\mu_i = \frac{V\kappa}{\alpha_0 P} \quad , \qquad \mu = \frac{V\kappa}{\alpha_0 Q} \, . \tag{30}$$

According to (22, 8) the [001] orientation is better than [111]. In (Khazanov et al., 2002b) it was shown that [001] is the best orientation.
The absorption coefficient α_0 at 1064nm wavelength in TGG can vary by several times from sample to sample, see Table 1, where values of V and κ are also included. The most likely value of κ lies in the range 4-5W/Km. Direct measurements of ξ, P and Q were not done because of difficulty in measuring the photoelastic coefficients p_{ij}. The results of measurements by means of techniques based on thermal effects are shown in Table 1.
As can be seen from expressions (30), and from Table 1, the TGG crystal has a considerable advantage over all glasses due to its high thermal conductivity. At the same time both Q and P can be effectively controlled in glasses by changing their content. For instance, among laser glasses there is a quartz neodymium glass having $Q=0.2\cdot10^{-7}K^{-1}$ (Demskaya & Prokhorova, 1983). If a magneto-optical glass with such a Q were created, its figure of merit μ would be better than in TGG.
Two other terbium garnets have V 35% higher than TGG: TAG (Ganschow et al., 1999; Rubinstein et al., 1964; Geho et al., 2005) and TSAG (Yoshikawa et al., 2002). Verdet constants of $LiTb(MoO_4)_2$ (Guo et al., 2009) and $NaTb(WO_4)_2$ (Liu et al., 2008) are even higher. However, the figures of merit μ_i and μ of all these crystals are unknown up to now. Besides, their diameters are a few mm only.
The greatest disadvantage of TGG is also a relatively small aperture (<30mm), whereas glasses can have a diameter as large as 300 mm. In (Khazanov, 2003; Khazanov, 2004) we proposed to use TGG polycrystalline ceramics in FIs. The first samples of TGG ceramics were made by Dr. A.Ikesue (Japan) in 2003, see Fig. 4, and the first experimental study was done in (Yasuhara et al., 2007). Also, ceramics may be made of other garnets and oxides:

TAG or TSAG (high V and κ) and highly (up to 20%) Nd-doped YAG, Y_2O_5, Sc_2O_5, Lu_2O_5 (low α_0 and high κ). We forecast that the use of FIs in lasers with high average power will expand considerably within the next few years due to the emergence of ceramics. In (Kagan & Khazanov, 2004) we studied specificity of thermal effects in magneto-optical ceramics and showed that figures of merit for ceramics are the same as for a single crystal with [111]-orientation.

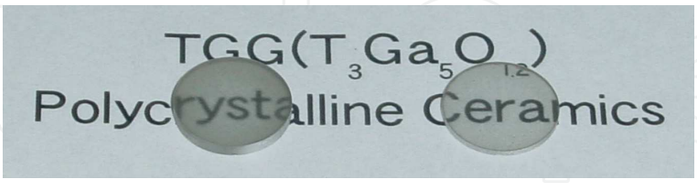

Fig. 4. A photograph of the first TGG ceramics samples made by A.Ikesue (Japan) in 2003.

3. Compensation of thermal effects in Faraday Isolators

3.1 Compensation of thermal lens in Faraday Isolators

The temperature distribution in the MOE and, consequently, the distribution of phase of an aberrated laser beam are almost parabolic. Therefore, a great portion of the phase distortions can be compensated by means of an ordinary lens or a telescope (Khazanov, 2000) shown by a dashed line in Fig. 5. Hereinafter we shall call this method "telescopic compensation" and indicate corresponding losses by subscript "TC".

In (Mansell et al., 2001; Mueller et al., 2002) an adaptive method (subscript "AC") for compensating the thermal lens was suggested and experimentally studied. A compensating glass was placed before polarizer 1 (dotted line in Fig. 5). Parameters of the compensating glass were chosen so that the thermal lens had the same focus as in FI but opposite (typically negative) sign. In (Mueller et al., 2002) it was shown numerically that the influence of diffraction can be insignificant. In this case the isotropic losses were totally compensated: $\gamma_{iAC}=0$.

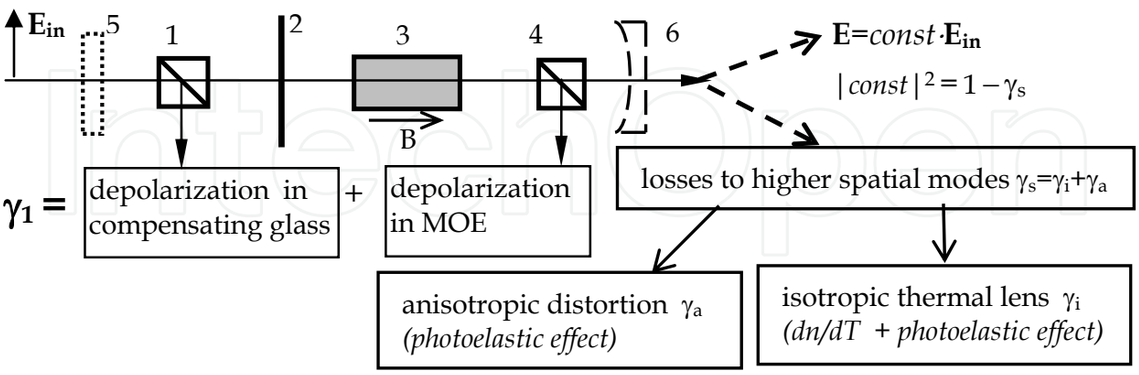

Fig. 5. Power losses during first propagation through FI. 1,4 – polarizers; 2 – $\lambda/2$ plate; 3 – MOE, 5 – compensating glass, 6 – compensating lens or telescope.

The adaptive approach has two certain advantages over the telescopic one: there is no need in adjustment when laser power is changed, and the accuracy of compensation is higher. However, a considerable disadvantage of the adaptive method is that the photoelastic effect

in the compensating glass leads to additional (besides isotropic) distortions and, consequently, to losses in the spatial polarization mode. Thus, the above two methods can compensate only for γ_i . The telescopic method is less efficient but does not lead to increase of losses γ_1 and γ_a. The adaptive method totally compensates for γ_i but increases losses γ_1 and γ_a because of the photoelastic effect in the compensating glass, which has not been considered in (Mueller et al., 2002).

In (Khazanov et al., 2004) a detailed theoretical analysis of the two compensation methods is presented. Analytical expressions for all γ are summarized in Table 3. These formulas are valid when $\theta=\theta_{opt}$, condition (18) is obeyed, and phase distortions are weak. Parameter p_{CG} is defined by (11), with all material constants for compensating glass.

As one can see from Table 3, the losses associated with isotropic thermal lens γ_i can be reduced by the telescopic method by $A_3/A_4 \cong 15$ times, as was shown in (Khazanov, 2000). In (Mueller et al., 2002; Mansell et al., 2001) this value appeared to be twice as small as it should be because of mistake made in the calculations.

For a super-Gaussian beam (29), all the formulas in Table 3 are valid if A_i is replaced by $A_i(m)$, expressions for which are given in Table 2. The $A_3(m)/A_4(m)$ ratio grows with increasing m, i.e. the compensation of isotropic thermal lens induced by a super-Gaussian beam is more efficient. In particular, for a flat-top beam the isotropic thermal lens can be totally compensated – $A_4(\infty)=0$. This has a simple physical explanation: at a uniform heat release there is a strictly parabolic temperature distribution in a rod.

A key parameter of the compensating glass is the P_{CG}/Q_{CG} ratio, and the higher this ratio, the better the glass (Khazanov et al., 2004). Specifically, an increase of γ_1 and γ_a by glass is rather small if $P_{CG}/Q_{CG}>10$ and may be neglected if $P_{CG}/Q_{CG}>50$. The thermal lens averaged for two polarizations was almost totally compensated by means of FK51 Schott glass in (Khazanov et al., 2004): the difference of the phase from a constant was reduced from 0.9 to 0.02 radian. At the same time, the astigmatism of the resulting lens was very large, because of the small ratio $P_{FK51}/Q_{FK51}=2.8$.

The photoelastic effect can be totally compensated by using gel instead of glass, as it is done for compensation of thermal lens in laser amplifiers (Roth et al., 2004). Another approach is to use a crystal with natural birefringence, in which the thermally induced birefringence may be neglected. Examples are YLF, KDP, DKDP, LiCAF.

A 5.5-mm-thick DKDP crystal was successfully used in (Zelenogorsky et al., 2007). 2D phase maps are shown in Fig. 6. It was demonstrated in experiment that for 45 W laser power the compensation allows reducing power losses in Gaussian mode γ_s from 26% to 0.5%. Calculations have shown that losses can be reduced to a level of 4.7%, even for a laser power of 150 W. At present, a DKDP crystal seems to be the best choice for adaptive thermal lens compensation and is widely used in FI in high average power lasers.

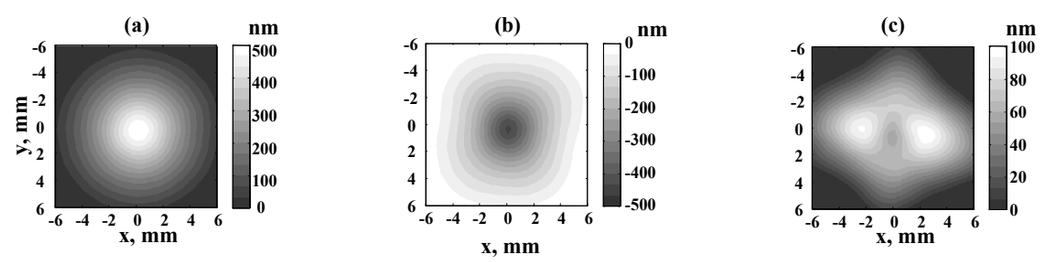

Fig. 6. Thermally induced phase map for FI (a), DKDP (b), and both FI and DKDP (c).

3.2 Depolarization compensation in FI with one magneto-optical element

The idea (Andreev et al., 2002) consists in creating a phase plate, in which all phase incursions that a beam assumes in the MOE are subtracted. For this, the phase plate should have the same transverse distribution of eigen polarizations and phase shift as in the MOE, except that the phase shift is opposite in sign. In this case, the radiation, having successively passed through these two elements, keeps its initial polarization unaltered. If the phase plate is reciprocal, then the non-reciprocal properties of the FI (rotation of polarization by 90^0 during two passes) are maintained.

In a MOE made of glass (ξ=1) or a cubic crystal with the [111] orientation one can derive from (3-7) that $\Psi=\varphi$ and δ_l does not depend on φ and near the beam axis $\delta_l \sim r^2$ (this is not so for crystals with other orientations, but we shall not consider such cases in this section). When a plane wave propagates in crystalline quartz at an angle $\Phi<<1$ relative to the optical axis, there is also superposition of linear and circular birefringences. The phase shift of linear birefringence $\delta_{ql} \sim \Phi^2$. At propagation of a converging or diverging beam (Fig. 7) the angle Φ is proportional to r, i.e., $\delta_{ql} \sim r^2$, and the inclination angle of eigen polarization of the linear birefringence is equal to φ. Therefore, if directions of polarization rotation in the MOE and quartz rotator (QR) are opposite (i.e., $\delta_c=-\delta_{qc}$), then the compensation of depolarization after successive passes through the MOE and QR is possible.

A formula for depolarization ratio γ_q of FI in Fig. 7 was derived in (Andreev et al., 2002). γ_q depends on laser power P_0 and at optimal power has minimum γ_{qmin}:

$$\gamma_{q\min} = A_5(m)(1+2\xi)^2 p^2/(9\pi^2)\,. \tag{31}$$

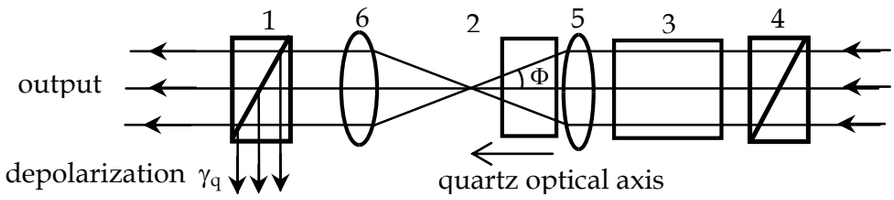

Fig. 7. Depolarization compensation in FI: 1,4 – polarizers, 2 – 45^0 QR, 3 – MOE, 5 and 6 – lenses of telescope. MOE and QR rotate in opposite directions.

Figure 8 shows experimental and theoretical plots for $\gamma(P_0)$ and $\gamma_q(P_0)$. At low power, the thermal effects are small, and the traditional design provides better isolation: $\gamma<\gamma_q$. When power is increased, γ_q decreases reaching its minimum value γ_{qmin}. Without compensation the theory is in good agreement with experiment at high powers, when γ is much greater than the "cold" depolarization ratio $\gamma_{cold}=2.5\cdot10^{-4}$. At the focal length of lens 5 f=125mm, the experimental value of γ_{qmin} is considerably greater than the theoretical prediction because γ_{cold} is 2.5 times as great as the theoretical value of γ_{qmin} for this case. At high powers, $\gamma_{cold}<<\gamma_q$ and theoretical and experimental values of γ_q coincide. At f=88mm experimental values of γ_q are higher than the theoretical ones, but the difference is not crucial.

Of major interest from a practical standpoint is the γ/γ_{qmin} ratio which shows by how many times the isolation degree can be more when the design in Fig. 7 is used. From (22, 31), with (8) taken into account, for the [111] orientation we obtain $\gamma/\gamma_{qmin}=A_1(m)/A_5(m)$; and this ratio increases with increasing m, see Table 2. In experiment (see Fig. 8) $A_1(1)/A_5(1)=8$ instead of

the theoretically predicted 11.5. This difference is attributed to some ellipticity of the beam and non-ideal coaxiality of lens 3 and the beam.

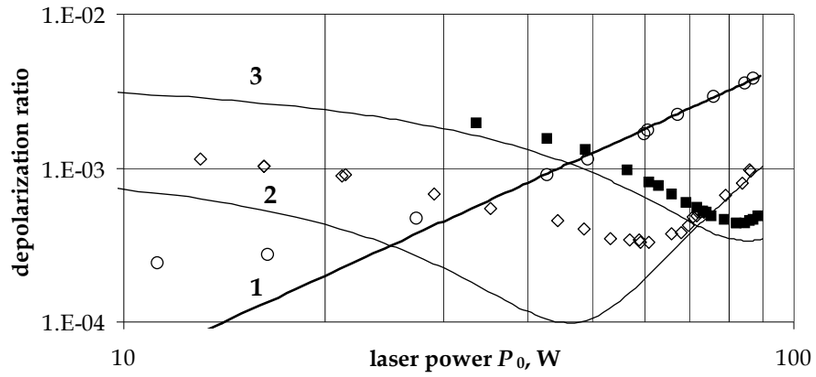

Fig. 8. Depolarization ratio in traditional FI design $\gamma(P_0)$ (curve 1, circles) and design in Fig. 7 $\gamma_q(P_0)$ at f=125mm (curve 2, rhombs) and f=88mm (curve 3, squares) (Andreev et al., 2002).

The main advantage of the design in Fig. 7 is a possibility to upgrade a standard commercial FI without re-assembling its magnetic system. The designs comprising two magneto-optical elements require a special magnetic system but they are more efficient and useful in practice, as will be discussed in the next section.

3.3 Depolarization compensation in Faraday isolators with two magneto-optical elements

It is well known that a 90^0 polarization rotator placed between two identical phase plates with linear eigen polarizations provides total compensation of birefringence (Scott & de Wit, 1971). If there is also circular birefringence in these plates, this statement is valid only when the directions of rotation of the polarization plane in the plates are different. It is however unacceptable for FI, because in this case it loses nonreciprocal properties. Nevertheless, replacing one 45^0 MOE by two 22.5^0 MOEs with a reciprocal optical element between them (a $\lambda/2$ plate or a QR as shown in Fig. 9) compensates depolarization (Khazanov, 1999).

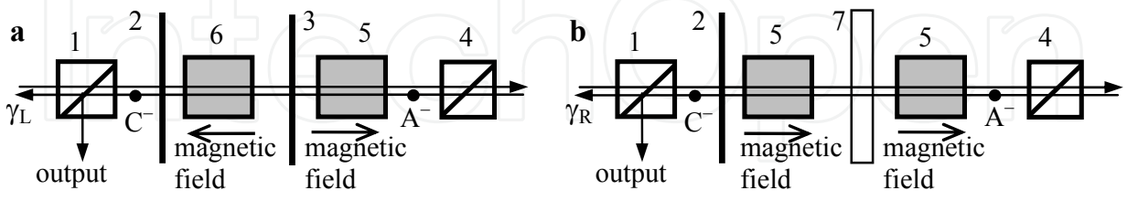

Fig. 9. FI designs with a $\lambda/2$ plate (a) and QR (b) (Khazanov, 1999). 1,4 – polarizers, 2,3 – $\lambda/2$ plates, 5 – 22.5^0 MOE rotating clockwise, 6 – 22.5^0 MOE rotating anticlockwise, 7 – 67.5^0 QR.

Let us find γ_L and γ_R for the novel designs (subscripts "L" and "R" will denote FI designs illustrated in Fig. 9a and 9b, respectively). The field **E** at a point C^- can be easily found:

$$\mathbf{E}_L(C^-) = \mathbf{L_2}(\beta_L+\pi/8)\mathbf{F}(\delta_c=-\pi/4, \delta_l/2)\mathbf{L_2}(\beta_L)\mathbf{F}(\delta_c=\pi/4, \delta_l/2)\mathbf{E}(A^-), \quad (32)$$

$$\mathbf{E}_R(C^-) = \mathbf{L_2}(\beta_R/2+3\pi/8)\mathbf{F}(\delta_c=\pi/4, \delta_l/2)\mathbf{R}(\beta_R)\mathbf{F}(\delta_c=\pi/4, \delta_l/2)\mathbf{E}(A^-)\,, \tag{33}$$

where **F** and $\mathbf{L}_2$ are defined by (1, 17), $\mathbf{R}(\beta_R)$ is the matrix of QR (matrix of rotation by an angle β_R). We assume that the phase shift of the linear birefringence in each MOE is $\delta_l/2$, i.e. δ_l is the phase incursion for an entire pass through FI for all designs in Figs. 1 and 9. In the approximation (18**)** the substitution (32, 33) into (14) instead of $\mathbf{E}_C$ yields the expressions for $\gamma_{L,R}$. From these expressions it can be seen that at

$$\beta_L=\beta_{optL}=\pi/8+j\pi/2 \qquad \beta_R=\beta_{optR}=3\pi/8+j\pi \tag{34}$$

(j is an integer) $\gamma_{L,R}$ become proportional to the fourth power of δ_l, whereas γ (22) is proportional to the second power of δ_l. Taking into account (18), this indicates that for (34) $\gamma_{L,R}<<\gamma$, i.e. the isolation degree increases considerably in the two novel designs (Fig. 9) in comparison with the traditional one (Fig. 1). If (34) is valid,

$$\gamma_L(\theta) = p^4 A_2 \pi^{-4}\left[6a^2\left(1+\frac{2}{3}\xi^2+\xi^4\right)+8b^2\xi^2+6b^2\left(1-\xi^2\right)^2\sin^2\theta_4-12ab\left(\xi^4-1\right)\sin\theta_4\right], \tag{35}$$

$$\gamma_R = p^4 6a^2 A_2 \pi^{-4}\left(1+2\xi^2/3+\xi^4\right), \tag{36}$$

where $\theta_4=4\theta-\pi/4$, $a=(\pi-2\sqrt{2})/8$, $b=(2-\sqrt{2})/4$. Note that γ_R does not depend on angle θ at all, whereas γ_L depends on it. By varying angle θ (in practice by rotating both MOEs around the *z* axis) it is possible to find θ_{opt} and minimal value of the depolarization ratio γ_L:

$$\theta_{optL} = \frac{\pi}{16}+\frac{1}{4}\mathrm{Re}\left\{\arcsin\left[\frac{a}{b}\cdot\frac{\xi^2+1}{\xi^2-1}\right]\right\} \tag{37}$$

$$\gamma_L = \gamma_L(\theta=\theta_{optL}) = \begin{cases} p^4 8A_2\pi^{-4}\xi^2\left(b^2-a^2\right) & \xi>1.315 \quad \xi<0.760 \\ p^4 2A_2\pi^{-4}\left[3(a+b)^2+2\xi^2(a^2-b^2)+3\xi^4(a-b)^2\right] & 1\le\xi<1.315 \\ p^4 2A_2\pi^{-4}\left[3(a-b)^2+2\xi^2(a^2-b^2)+3\xi^4(a+b)^2\right] & 0.760<\xi\le 1 \end{cases} \tag{38}$$

Thus, $\gamma_{L,R}$ are determined, like γ in the traditional design, only by two parameters: p and ξ. The polarization distortions which a beam acquires when passing through the first MOE, are compensated, though not totally as in laser amplifiers (Scott & de Wit, 1971), but rather partially yet efficiently when passing through the second MOE. For a super-Gaussian beam (29) one can easily show that formulas (34-38) remain valid at any m, if A_2 is replaced by $A_2(m)$.

Formulas (36,38) are valid if condition (18) is obeyed. In a general case, analytical expressions cannot be obtained. Numerical integration showed that β_{optR} and β_{optL}, like at $\delta_l<<1$, are determined by expressions (34). Figure 10 presents the plots of $\gamma(p)$ for all the three designs. A considerable decrease of the depolarization ratio in both novel designs persists even when the condition (18) is disobeyed. It can be seen from Fig. 10 that the design with QR (Fig. 9a) provides better isolation degree than the design with a $\lambda/2$ plate (Fig. 9b). At the same time, we should note an important advantage of the design with a $\lambda/2$ plate: the different direction of polarization rotation in the MOEs and, consequently,

different direction of the magnetic field. With an appropriate arrangement of the magnetic system, this reduces the total length of MOEs L (Shiraishi et al., 1986) and leads to an additional decrease in γ_L, which is proportional to L^4.

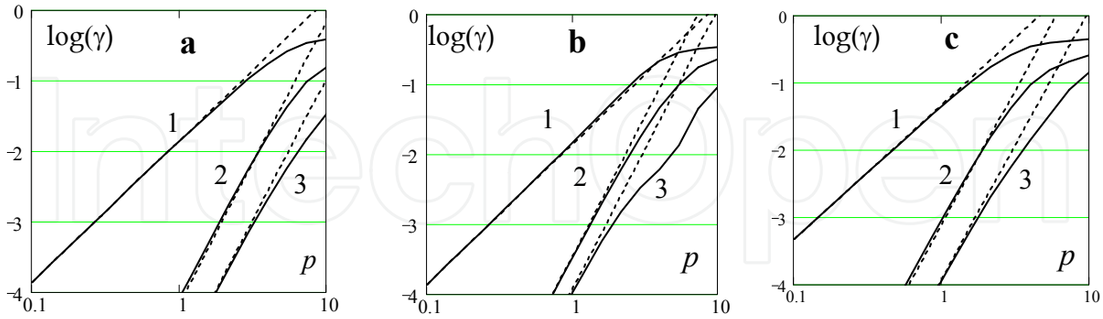

Fig. 10. Numerical (solid curves) and analytical (22, 36, 38) (dashed) plots of $\gamma(p)$ for the traditional FI design in Fig. 1 (1), $\gamma_L(p)$ for FI design with a $\lambda/2$ plate in Fig. 9a (2), and $\gamma_R(p)$ for FI design with QR in Fig 9b (3). (a) glass (b) TGG crystal with the [001] orientation, and (c) TGG crystal with the [111] orientation.

It can be seen from (36) that for TGG (ξ=2.25) γ_R is almost equal for the [001] and [111] orientations; any other orientation is worse (Khazanov et al., 2002a). At the same time, the [111] orientation does not require any mutual alignment of two MOEs. Thus, for the design in Fig. 9b the [111] orientation is more practical.

Power losses during the first passes through the FI designs in Fig. 9 can be calculated using the procedure described in section 2.3 (Khazanov, 2000). The results are summarized in Table 3. As can be expected, γ_i is the same for all three designs. With regard to minimization (γ_a+γ_1), both novel designs are slightly better than the traditional one.

The efficiency of depolarization compensation in the novel designs was first experimentally confirmed for MOEs made of glass (Khazanov et al., 2000). Experimental results for TGG-based FI with QR are summarized in Fig. 11. The first test (rhombs, total TGG crystals length 22mm, diameter 11mm) showed excellent compensation of thermal effects and 45dB isolation at up to 90W power. The most powerful experiments (circles, total TGG crystals

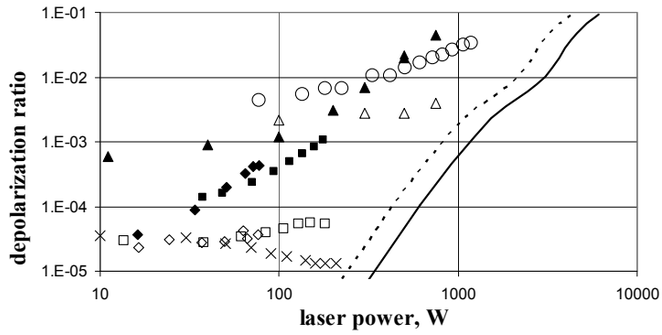

Fig. 11. Experimental plots of $\gamma(P_0)$ (filled symbol) and $\gamma_R(P_0)$ (open symbol) for different FIs: (Andreev et al., 2000b) (rhombs), (Nicklaus et al., 2006) (circles), (Voytovich et al., 2007) (squares, triangles), and unpublished data (crosses). Theoretical curves correspond to $\gamma_R(P_0)$ for squares (solid) and triangles (dashed).

length 15mm, aperture 4x8mm) showed depolarization much worse than the theoretical predictions due to bad crystal quality and non-optimized alignment. Three 20mm-diameter FIs with total TGG crystals length 18mm (triangles, squares, and crosses) showed at least an order of magnitude compensation of depolarization. Isolation degrees (24dB, 42dB, and 49dB) are mostly defined by cold depolarization. Theoretical curves show that these FIs provide more than 20 dB isolation at laser power up to 3kW. Nowadays the FIs with QR (Fig. 9b) are widely used in high average power lasers.

4. Suppression of thermal effects in Faraday Isolators

4.1 Cryogenic Faraday isolators

In (Zheleznov et al., 2006) we suggested cooling FI to liquid nitrogen temperature to improve the high average power characteristics. The Verdet constant and the magnetic field grow when temperature decreases, so the length of the MOE becomes shorter and hence the isolation degree $1/\gamma$ increases. Also, thermo-optical properties of TGG and magneto-optical glasses are improved at nitrogen temperature. All this aspects allow drastically suppressing all thermal effects. Let us discuss it in details.

It is known (Zarubina et al., 1987; Barnes & Petway, 1992; Davis & Bunch, 1984) that the Verdet constant of TGG and magneto-optical glasses depends on temperature according to the law V=const/T. Recent studies (Yasuhara et al., 2007) confirm this dependence for TGG-ceramics too. Therefore, cooling MOE to 77K will make it possible to reduce its length almost by a factor of 4.

Magnetic field also grows when the magnetic system is cooled. But the most frequently used Nd-Fe-B magnet showed second-order phase transition at T>135K; consequently, magnetic field at 77K depends on cooling speed (Zheleznov et al., 2007). In that paper we also showed that there is no phase transition in samarium-cobalt alloy (Sm-Co) magnets and that magnetic field at 77K is lager than at 300K by a factor of 1.2 and does not depend on cooling speed. So, in cryogenic FIs the Sm-Co magnets may be more efficient, even though they are weaker than Nd-Fe-B.

Temperature dependence of the depolarization ratio γ and thermal lens in TGG and magneto-optical glass MOC-04 were measured in (Zheleznov et al., 2006). As temperature was reduced to 102K the focal length F increased by a factor of 2.7 (Fig. 12a), allowing us to expect a 3.6 times increase at 77K. Formulas (27,28) show that this corresponds to a 3.6 times decrease of parameter $\alpha P/\kappa$. Reduction of this parameter for MOC-04 glass is about a factor of 1.8.

At 86K, γ in TGG decreased 8-fold, see Fig. 12b. At 77K, we can expect a decrease by a factor more than 9. Therefore, a decrease of parameter $\alpha Q/\kappa$ by a factor of 3 follows from expressions (22, 11). This TGG crystal was grown from a melt. The thermal conductivity of such crystals in the temperature range from 77K to 300K is almost constant (Slack & Oliver, 1971), so the measured decrease of γ is related to decreasing αQ.

Let us estimate the maximum average power of the FI cooled to 77K. According to (22, 11), at a given value of γ the laser power P_0 is proportional to $\kappa/\alpha QL$. Since parameter αQ is about three times lower and the growth of the Verdet constant and the magnetic field allow a 5-fold reduction of the crystal length L, P_0 will be increased by a factor of 15. Use of flux-grown TGG crystals allows further doubling of the laser power because the thermal conductivity of such crystals is twice as great at 77K (Slack & Oliver, 1971). This allows using traditional FI (Fig. 1) at the laser power up to 10kW.

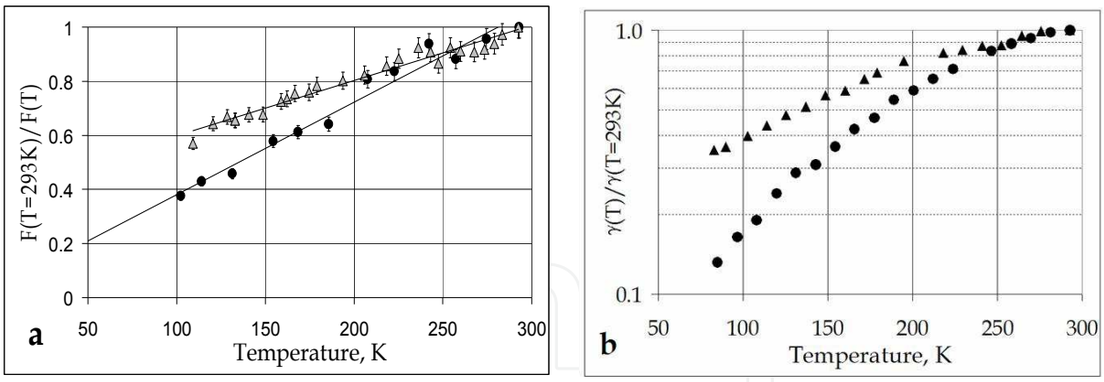

Fig. 12. Temperature dependence of the focal length of thermal lens F (a) and depolarization γ (b) in the TGG with the [001] orientation (circles, $F(T=293\text{K})=191\text{cm}$, $\gamma(T=293\text{K})=5.2\cdot10^{-3}$) and in glass MOC-04 (triangles, $F(T=293\text{K})=581\text{cm}$, $\gamma(T=293\text{K})=5.1\cdot10^{-3}$).

Traditional (Fig. 1) FI based on [111]-oriented TGG and FIs with QR (Fig. 9b) enjoy also the effect of ξ decreased by a factor of 1.9 (see Fig. 13b), i.e. from 2.25 to 1.2. According to (8,22) and (36) this increases maximum power by a factor of 1.6 in both cases. Bearing in mind that FIs with QR at room temperature can operate at 1-2kW, we obtain that at T=77K the maximum power will be tens of kW. Since the P/Q ratio is little dependent on temperature (Fig. 13a), all the above considerations are valid for both, the isolation and the thermal lens.
Note that in cryogenic FIs the temperature dependence of Verdet constant becomes more important because of increasing $V^{-1}\mathrm{d}V/\mathrm{d}T$ and deceasing L; compare two terms in (21**)**. In order to suppress the $\mathrm{d}V/\mathrm{d}T$ effect it is promising to cool TGG(s) through optical surfaces by means of a sapphire, for example (the characteristic length of the TGG crystal(s) in cryogenic FIs is about 3mm). Advantages of such disk geometry (see section 4.3) are huge reduction of depolarization caused by both, temperature dependence of Verdet constant and photoelastic effect. Our recent study showed that FI cooling is a very promising technique, which had been successfully applied in laser amplifiers (Ripin et al., 2004).

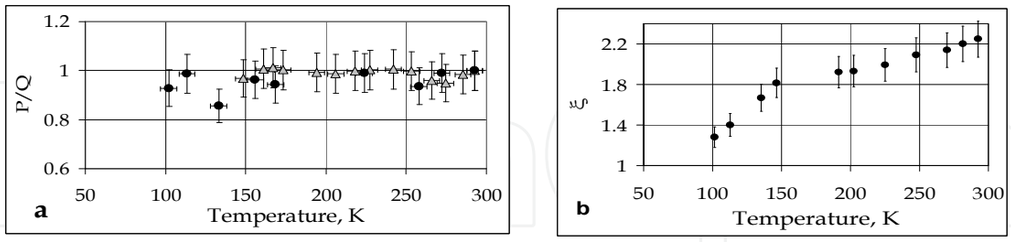

Fig. 13. Temperature dependence of the P/Q ratio (a) and parameter of optical anisotropy ξ (b) for TGG (circles) and glass MOC-04 (triangles).

4.2 Increase of magnetic field of permanent magnets

An obvious way to increase laser power keeping the same isolation degree is to increase magnetic filed B, and hence to decrease MOE length L. In (Zheleznov et al., 2007) we describe experiments with magnetic systems based on superconducting solenoids with B=5T. Such a strong field opens one more approach to suppress the thermal effects: use new magneto-optical media with lower absorption and higher thermal conductivity, for example

YAG and GGG crystals with or without doping. Additional advantage of these crystals is huge increase of their thermal conductivity at 77K, see section 4.1.

Increasing of B is also possible for a magnetic system based on constant magnets, even though it is a complex task. First, an increase of B implies shortening of the MOE, which imposes additional requirements to transverse homogeneity of B. Second, an increase of B demands building-up a mass of magnets and reinforces the mutual demagnetizing action of the neighboring magnets. Moreover, when the required (calculated) distribution of magnetization vector is achieved, one has to overcome technological difficulties at the stage of production and assembling.

In (Gauthier et al., 1986; Shiraishi et al., 1986) magnetic systems with a magnetic field up to 1T were designed. Typically a magnetic system is a set of axially and radially magnetized rings (Geho et al., 2005). The calculations demonstrated that such a system made it possible to form a magnetic field up to 1.7 T (Mukhin et al., 2009). In that paper we also proposed to replace part of the magnets by a magnetic conductor, see Fig. 14. The total energy of the field of magnets decreases, but careful selection of the shape and position of the magnetic conductor allows a local increase of field intensity in TGG.

The magnetic conductor (made of steel) consisted of two parts: the external part that was a screen (Fig. 14d) closing magnetic lines of force of the poles of radially magnetized rings, and the internal part – a pole terminal (Fig. 14e) concentrating magnetic field lines near the TGG. The magnets were made of the Nd-Fe-B alloy: radially magnetized rings with residual induction B_{r1}=12 kGauss and coercitive magnetization force H_{c1}=13 kOe and axially magnetized ring (B_{r2}=10 kGauss, H_{c2}=27 kOe). The magnetic conductor increased the field in the center of the magnetic system from 1.7 T to 2.1 T. Such a strong magnetic field enabled creating a 13mm-diameter FI with the TGG length of only 10.3 mm at modest mass and size of the magnetic system (diameter 132 mm, length 140 mm, mass 12 kg).

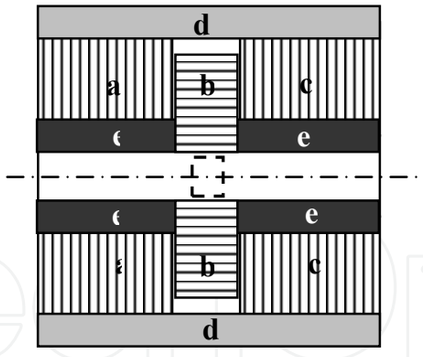

Fig. 14. Design of a magnetic system with B=2.1T: **a, c,** (**b)** are radially (axially) magnetized rings; **d,e** are magnetic conductor. Dashed rectangle shows TGG crystal.

In practice γ is determined by both, heat effects and "cold" depolarization. The latter depends on the TGG quality and magnetic field inhomogeneity. Note that the magnetic conductor also decreases inhomogeneity down to <0.3%, which corresponds to cold depolarization 50dB. In terms of maximal operating power, our FI (Mukhin et al., 2009) is 3…5 times better than the FI manufactured by leading companies and provides the isolation degree of ~30 dB at average laser power of ~400 W, see Fig. 15. Such a high power is ensured by a homogeneous magnetic field of 2.1 T (and, hence, a short TGG), as well as by the [001] orientation of a TGG crystal instead of [111], see (22, 8).

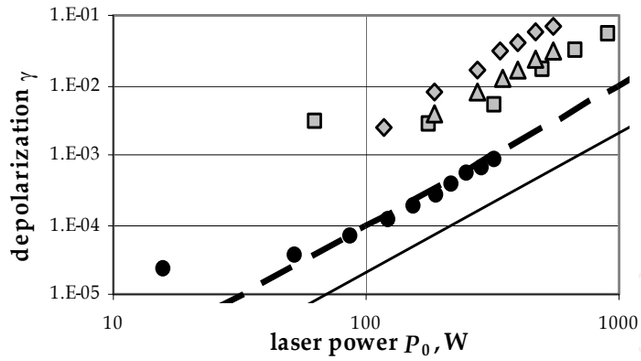

Fig. 15. γ as a function of P_0 for FI with B=2.1T (Mukhin et al., 2009) (circles, dashed line is theory for $\alpha=2.5\cdot10^{-3}\text{cm}^{-1}$), and for commercial FIs (Nicklaus et al., 2006) produced by Litton (rhombs), Linos (triangles), and EOT (squares). Solid line is theory for FI with B=2.5T and $\alpha=1.5\cdot10^{-3}\text{cm}^{-1}$.

If still stronger magnets are used, it will be possible to make TGG still shorter and to additionally increase admissible optical power. The estimates demonstrated a feasibility of producing FI with TGG 13 mm in diameter and 7 mm long using magnets with the following parameters: B_{r1}=14 kGauss, H_{c1}=16 κOe; B_{r2}=11.2 kGauss, H_{c2}=35 kOe. Recent experiments (Palashov et al., 2009) showed a possibility to reach B=2.5T and to shorten TGG to 8mm. If TGG with small absorption ($\alpha=1.5\cdot10^{-3}$ cm^{-1}) is used, the FI provides 27 dB isolation degree at laser power 1 kW, see Fig. 15. According to (28, 27), the thermal lens focal length in this FI will be 19m at 1kW (we assume the Gaussian beam radius r_0 to be 2.5 mm). The lens may be compensated as discussed in section 3.1.

4.3 Faraday isolators based on slab and disc geometries

Above we considered rod MOE geometry. Use of either slabs or several thin discs (Fig. 16) is more attractive for the thermal effects suppression. In this section we shall study these geometries both for traditional (Fig. 1) and novel (Fig. 9) FI designs. We shall focus on two main questions: how the depolarization depends on the aspect ratio of slab or disc, and what yield in maximum power the novel designs provide in comparison with the traditional one.

For slab geometry we shall use the following assumptions. The laser beam has a uniform intensity distribution over slab aperture and linear polarization along the x axis. Heat is removed only through horizontal surfaces, see Fig. 16a. The ratio of the slab thickness t to the slab width w is small: $R_s=w/t<<1$. Under these conditions, eigen polarizations of the birefringence induced by the photoelastic effect are oriented along the x and y axes, i.e. the matrix of MOE is described by formula (1) at Ψ=0. An expression for the phase shift δ_l is found in (Dianov, 1971):

$$\delta_l = \pi \frac{p}{R_s}\left(\frac{1}{6}-\frac{2y^2}{t^2}\right). \tag{39}$$

It is evident from (39) and the transition rule (8) that the [001] orientation provides a lower depolarization ratio. For the case (18) we derived the following formulas using the same mathematical procedure as for rod geometry (Khazanov, 2004):

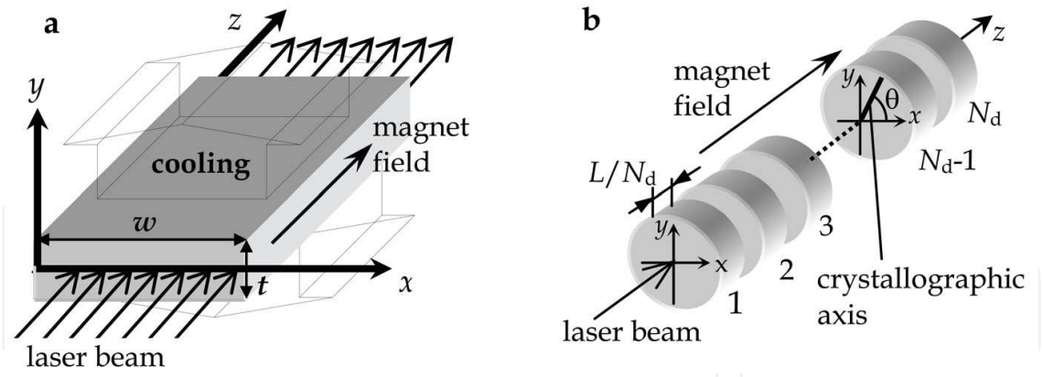

Fig. 16. Use of slabs (a) or discs (b) in Faraday isolators.

$$\gamma_{slab} = R_s^{-2} p^2 / 45 \quad \gamma_{slabL} = R_s^{-4} p^4 \left(\pi - 4\sqrt{2} + 2\right)^2 / 3780 \quad \gamma_{slabR} = R_s^{-4} p^4 \left(\pi - 2\sqrt{2}\right)^2 / 3780 . \qquad (40)$$

Numerical calculations made for an arbitrary aspect ratio R_s show that formulas (40) are valid at R_s>3. In practice, as a rule, R_s>3. Figure 17a presents the plot for $\gamma(p)$, both for rods and slabs. In practice, necessary values of the depolarization ratio usually lie within 10^{-4}–10^{-2}, where analytical formulas (40) are very accurate as seen from Fig. 17a.

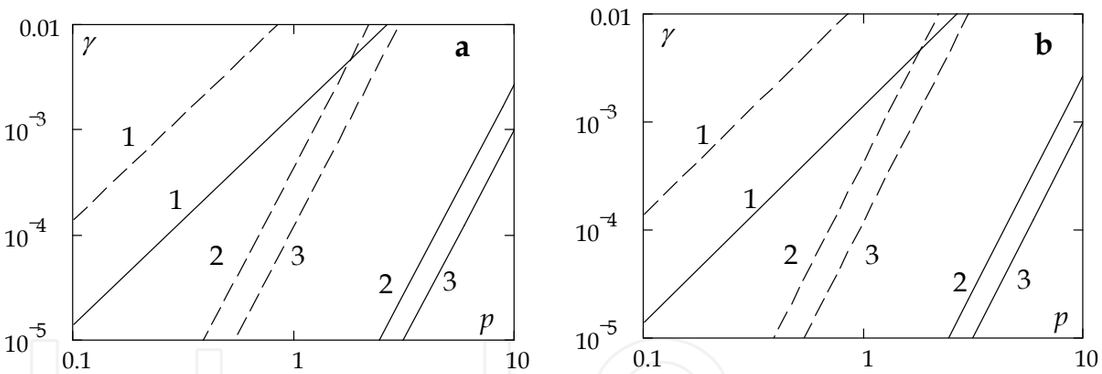

Fig. 17. The plots (solid lines) of $\gamma_{slab}(p)$ for TGG-based FI with slab, R_s=4 (a) and $\gamma_{disc}(p)$ for glass-based FI with discs, R_d=1.8 (b). 1 - FI design in Fig. 1; 2 – FI design in Fig. 9a; 3 – FI design in Fig 9b. Dashed lines show γ as a function of p for rods.

For all the FI designs shown in Figs. 1 and 9, $\gamma_{slab} << \gamma$. The depolarization ratio γ_{slab} is inversely proportional to the second power of the aspect ratio R_s for the traditional design, and to the fourth power of R_s for novel designs of FI. The depolarization ratio in novel designs is much lower than in the traditional one.

For TGG, ξ=2.25 and as follows from (40, 8), the [001] orientation provides a depolarization ratio that is 3.4 (11.3) times as small as that with the [111] orientation for the traditional (novel) designs. Estimations show that the FI presented in Fig. 9b with slabs made of TGG with aspect ratio R_s=5 at laser power 10kW provides an isolation degree of 30 dB. Slab-based FIs are used in high power slab lasers.

The idea of using thin discs consists in intensive cooling of optical surfaces (Fig. 16b). In this case the radial temperature gradient (the source of depolarization) will be considerably lower. At the same value of the magnetic field, the total length of magneto-optical elements L should be the same as in the rod geometry, i.e., N_d discs having length $h=L/N_d$ each should be used. Different relations between h, r_0 and disc radius R were considered in detail in (Mukhin & Khazanov, 2004), where it was shown that the analytical expressions obtained for the simplest case of thin ($h<<r_0$) and wide-aperture ($r_0<<R$) disc are valid if $R_d>3$, where $R_d= r_0/h$ is disc aspect ratio. In this case for $\theta=\theta_{opt}$ we have

$$\gamma_{disc}=\frac{A_6}{9\pi^2}(1-\nu)^2\frac{p^2}{R_d^4}\quad \gamma_{discL}=\frac{8A_7}{(3\pi)^4}(1-\nu)^4\xi^2\left(2a^2+b^2\right)\frac{p^4}{R_d^8}\quad \gamma_{discR}=\frac{2a^2A_7}{(3\pi)^4}(1-\nu)^4\left(3+2\xi^2+3\xi^4\right)\frac{p^4}{R_d^8} \quad (41)$$

As shown in (Mukhin & Khazanov, 2004), depolarization induced by temperature dependence of Verdet constant is less than γ_{disc} by four orders of magnitude. It is seen from (41) that when the disc thickness is reduced or the beam radius is increased, γ_{disc} drops in all cases. However, creation of thin discs involves engineering problems, see details in (Mukhin & Khazanov, 2004; Yasuhara et al., 2005). Therefore, it is reasonable to use the disc geometry for wide-aperture FIs. Such devices cannot be made of a TGG single crystal. However, magneto-optical glasses and TGG ceramics can be readily employed for this purpose. Figure 17b presents plots of $\gamma_{disc}(p)$ for rods and for discs made of magneto-optical glass ($\xi=1$).

Thus, γ_{disc} is inversely proportional to the fourth power of the aspect ratio R_d for the traditional design (Fig. 1), and to the eighth power of R_d for novel designs (Fig. 9). When discs are used instead of rods, the depolarization ratio can be reduced considerably if the disc thickness is less than the beam radius.

Estimations based on constants for magneto-optical glass (Table 1) show that when $R_d=2.5$ the FI presented in Fig. 9b provides an isolation degree of 35 dB at 5kW laser power. Use of TGG single crystal or TGG-ceramics allows using even higher power.

The disc geometry has two major disadvantages: optical surfaces have to be cooled, making the design more complicated and leading to wavefront distortions, and a large number of Fresnel back reflections; see details in (Mukhin & Khazanov, 2004).

5. Conclusion

Let us summarize the main results and discuss prospects for the future studies.

Thermal self-action of laser radiation in FIs leads to degradation of isolation degree $1/\gamma$ and to power losses in the initial spatial and polarization mode during the first pass through a FI. These losses comprise three components (Fig. 5): polarization losses γ_1, losses induced by isotropic thermal lens γ_i,, and losses associated with anisotropic amplitude-phase distortions γ_a. The isotropic thermal lens can be compensated, i.e. γ_i can be decreased by an ordinary negative lens or using an adaptive method with negative dn/dT compensator (DKDP crystal is the best choice). In the first case, γ_i can be reduced by a factor of 15. The adaptive method totally nulls γ_i , but increases γ_1 and γ_a. Formulas for all γ are summarized in Table 3.

The influence of the temperature dependence of the Verdet constant on the isolation degree $1/\gamma$ may be neglected as compared to the influence of the photoelastic effect. The FI design

comprising two magneto-optical elements (Fig. 9) and the design with a crystalline quartz in telescope (Fig. 7) provide depolarization compensation. The latter design has an advantage of using standard commercial FI. The most suitable for high power lasers is the FI design shown in Fig. 9b, which can provide 30dB isolation at an average power up to a few kWs.
Neither isolation degree nor power losses in initial Gaussian beam depend on beam radius, but they depend on beam shape. A flat-top shaped beam is optimal, whereas a Gaussian beam has the strongest self-action, see Table 2.
Slab and disk geometries (Fig. 16) allow increasing laser power in FI up to at least 10kW due to optimized thermal management. Note that the analysis presented in section 4.3 for a slab was made only for the [001] and [111] crystal orientations and only for incident polarization parallel to the slab edge. Therefore, additional four parameters appear (inclination angle of incident polarization and three Euler angles). By varying these parameters one can further increase the isolation degree.
Recently, magnetic field of constant magnets in FI was increased from 1T to 2T, thus shortening TGG to 10mm. Further increase up to 3T will probably be possible in the future. In spite of the practical disadvantages of the superconductive solenoids, they provide magnetic field up to 10T (TGG crystal is not cooled). Another approach is cooling the whole FI to 77K, because TGG figures of merit (30) improve drastically due to the Verdet constant and thermo-optical properties increase. In superconductive solenoids or at cooling to 77K the TGG crystal length is 2-3mm only. This allows implementing disc geometry with cooling through optical surfaces by means of sapphire, for example. As a result, in both cases FIs operating at giant average power of tens of kilowatts is possible.
Taking into account figures of merit of magneto-optical medium (30), the TGG crystal is the best choice for high average power lasers. For the FI shown in Fig. 1, the [001] orientation is the best (and [111] is the worst) of all possible orientations. For the FI design shown in Fig. 9b, isolation degree is the same for the [001] and [111] orientations, but the latter is more practical.
From the point of view of magneto-optical glass melting, the possibilities are far from being exhausted. The most promising idea is creation of athermal glass (similarly to available laser glasses), i.e. glass with low values of P and Q and as a result with figures of merit more than the TGG ones. New magneto-optical crystals, e.g., $LiTb(MoO_4)_2$ and $NaTb(WO_4)_2$ seem to be promising for the future developments.
In the nearest future we forecast wide usage of ceramics (TGG, TAG, TSAG, Nd-doped YAG, Y_2O_5, Sc_2O_5, Lu_2O_5, and others) due to its high thermal conductivity in comparison with glass, large aperture in comparison with single crystal, and low absorption.
Thus, even though up to now Faraday isolators were experimentally tested at average laser power of only 1kW, the 10-kilowatt barrier can be not only reached in the nearest future but also successfully overcome.

6. References

Andreev, N.; Babin, A.; Zarubina, T.; Kiselev, A.; Palashov, O.; Khazanov, E. & Shaveleov, O. (2000a). Thermooptical constant of magneto-active glasses. *Journal of Optical Technology*, Vol.67, No.6, (556-558), 1070-9762

Andreev, N.F.; Palashov, O.V.; Poteomkin, A.K.; Sergeev, A.M.; Khazanov, E.A. & Reitze, D.H. (2000b). A 45-dB Faraday isolator for 100-W average radiation power. *Quantum Electronics*, Vol.30, No.12, (1107-1108), 1063-7818

Andreev, N.F.; Katin, E.V.; Palashov, O.V.; Poteomkin, A.K.; Reitze, D.; Sergeev, A.M. & Khazanov, E.A. (2002). The use of crystalline quartz for compensation for thermally induced depolarization in Faraday isolators. *Quantum Electronics*, Vol.32, No.1, (91-94), 1063-7818

Barnes, N.P. & Petway, L.P. (1992). Variation of the Verdet constant with temperature of TGG. *Journal of the Optical Society of America B*, Vol.9, No.10, (1912-1915), 0740-3224

Carr, I.D. & Hanna, D.C. (1985). Performance of a Nd:YAG oscillator/amplifier with phase-conjugation via stimulated Brillouin scattering. *Applied Physics B*, Vol.36, No.2, (83-92), 0946-2171

Chen, X.; Lavorel, B.; Boquillon, J.P.; Saint-Loup, R. & Jannin, M. (1998). Letter: Optical rotary power at the resonance of the terbium $^7F_6 \rightarrow {}^5D_4$ line in terbium gallium garnet. *Solid-State Electronics*, Vol.42, No.9, (1765-1766), 0038-1101

Chen, X.; Galemezuk, R.; Salce, B.; Lavorel, B.; Akir, C. & Rajaonah, L. (1999). Long-transient conoscopic pattern technique. *Solid State Communications*, Vol.110, No.8, (431-434), 0038-1098

Davis, J.A. & Bunch, R.M. (1984). Temperature dependence of the Faraday rotation of Hoya FR-5 glass. *Applied Optics*, Vol.23, No.4, (633-636), 0003-6935

Demskaya, E.L. & Prokhorova, T.I. (1983). Investigation of properties of high-silica glass Nd_2O_3. *Fizika i Himiya Plasmi*, Vol.9, No.5, (554-560)

Denman, C.A. & Libby, S.I. (1999). Birefringence compensation using a single Nd:YAG rod. *Proceedings of Advanced Solid State Lasers,* pp. 608-612

Dianov, E.M. (1971). Thermal distortion of laser cavity in case of rectangular garnet slab. *Kratkiye Soobsheniya po Fisike*, Vol.8, (67-75), 1068-3356

Ganschow, S.; Klimm, D.; Reiche, P. & Uecker, R. (1999). On the crystallization of terbium aluminium garnet *Crystal Research and Technology*, Vol.34, No.5-6, (615-619), 0232-1300

Gauthier, D.J.; Narum, P. & Boyd, R.W. (1986). Simple, compact, high-performance permanent-magnet Faraday isolator. *Optics Letters*, Vol.11, No.10, (623-625), 0146-9592

Geho, M.; Takagi, T.; Chiku, S. & Fujii, T. (2005). Development of optical isolators for visible light using terbium aluminum garnet ($Tb_3Al_5O_{12}$) single crystals. *Japanese Journal of Applied Physics, Part 1*, Vol.44, No.7A, (4967-4970), 0021-4922

Gelikonov, V.M.; Gusovskii, D.D.; Leonov, V.I. & Novikov, M.A. (1987). Birefringence compensation in single-mode optical fibers. *Sov. Tech. Phys. Lett*, Vol.13, No.7, (322-323),

Giuliani, G. & Ristori, P. (1980). Polarization flip cavities: a new approach to laser resonators. *Optics Communications*, Vol.35, No.1, (109-112), 0030-4018

Guo, F.; Ru, J.; Li, H.; Zhuang, N.; Zhao, B. & Chen, J. (2009). Growth and magneto-optical properties of $LiTb(MoO_4)_2$ crystal. *Applied Physics B*, Vol.94, No.3, (437-441), 0946-2171

Ivanov, I.; Bulkanov, A.; Khazanov, E.; Mukhin, I.B.; Palashov, O.V.; Tsvetkov, V. & Popov, P. (2009). Terbium gallium garnet for high average power Faraday isolators: modern aspects of growing and characterization. *Proceedings of CLEO /EUROPE-EQEC 2009,* pp. CE.P.12 MON, Munich, Germany

Jiang, Y.; Myers, M.J. & Rhonenhouse, D. (1992). High Verdet constant Faraday rotator glasses. *SPIE Proceedings,* Vol.1761, (268-272), 9780819409348, Damage to Space Optics, and Properties and Characteristics of Optical Glass

Kagan, M.A. & Khazanov, E.A. (2004). Thermally induced birefringence in Faraday devices made from terbium gallium garnet-polycrystalline ceramics. *Applied Optics*, Vol.43, No.32, (6030-6039), 0003-6935

Kaminskii, A.A.; Eichler, H.J.; Reiche, P. & Uecker, R. (2005). SRS risk potential in Faraday rotator $Tb_3Ga_5O_{12}$ crystals for high-peak power laser. *Laser Physics Letters*, Vol.2, No.10, (489-492), 1612-2011

Khazanov, E.A. (1999). Compensation of thermally induced polarization distortions in Faraday isolators. *Quantum Electronics*, Vol.29, No.1, (59-64), 1063-7818

Khazanov, E.A.; Kulagin, O.V.; Yoshida, S.; Tanner, D. & Reitze, D. (1999). Investigation of self-induced depolarization of laser radiation in terbium gallium garnet. *IEEE Journal of Quantum Electronics*, Vol.35, No.8, (1116-1122), 0018-9197

Khazanov, E.A. (2000). Characteristic features of the operation of different designs of the Faraday isolator for a high average laser-radiation power. *Quantum Electronics*, Vol.30, No.2, (147-151), 1063-7818

Khazanov, E.; Andreev, N.; Babin, A.; Kiselev, A.; Palashov, O. & Reitze, D. (2000). Suppression of self-induced depolarization of high-power laser radiation in glass-based Faraday isolators. *Journal of the Optical Society of America B*, Vol.17, No.1, (99-102), 0740-3224

Khazanov, E.A. (2001). A new Faraday rotator for high average power lasers. *Quantum Electronics*, Vol.31, No.4, (351-356), 1063-7818

Khazanov, E.; Andreev, N.; Palashov, O.; Poteomkin, A.; Sergeev, A.; Mehl, O. & Reitze, D. (2002a). Effect of terbium gallium garnet crystal orientation on the isolation ratio of a Faraday isolator at high average power. *Applied Optics*, Vol.41, No.3, (483-492), 0003-6935

Khazanov, E.A.; Anastasiyev, A.A.; Andreev, N.F.; Voytovich, A. & Palashov, O.V. (2002b). Compensation of birefringence in active elements with a novel Faraday mirror operating at high average power. *Applied Optics*, Vol.41, No.15, (2947-2954), 0003-6935

Khazanov, E. (2003). Investigation of Faraday isolator and Faraday mirror designs for multi-kilowatt power lasers. *SPIE Proceedings,* Vol.4968, (115-126), 9780819447685, Solid State Lasers XII, San Jose, California

Khazanov, E. (2004). Slab-based Faraday isolators and Faraday mirrors for 10kW average laser power. *Applied Optics*, Vol.43, No.9, (1907-1913), 0003-6935

Khazanov, E.A.; Andreev, N.F.; Mal'shakov, A.N.; Palashov, O.V.; Poteomkin, A.K.; Sergeev, A.M.; Shaykin, A.A.; Zelenogorsky, V.V.; Ivanov, I.; Amin, R.S.; Mueller, G.; Tanner, D.B. & Reitze, D.H. (2004). Compensation of thermally induced modal

distortions in Faraday isolators. *IEEE Journal of Quantum Electronics*, Vol.40, No.10, (1500-1510), 0018-9197

Liu, J.; Guo, F.; Zhao, B.; Zhuang, N.; Chen, Y.; Gao, Z. & Chen, J. (2008). Growth and magneto-optical properties of $NaTb(WO_4)_2$. *Journal of Crystal Growth*, Vol.310, No.10, (2613-2616), 0022-0248

Malshakov, A.N.; Pasmanik, G. & Poteomkin, A.K. (1997). Comparative characteristics of magneto-optical materials. *Applied Optics*, Vol.36, No.25, (6403-6410), 0003-6935

Mansell, J.D.; Hennawi, J.; Gustafson, E.K.; Fejer, M.M.; Byer, R.L.; Clubley, D.; Yoshida, S. & Reitze, D.H. (2001). Evaluating the effect of transmissive optic thermal lensing on laser beam quality with a Shack-Hartmann wave-front sensor. *Applied Optics*, Vol.40, No.3, (366-374), 0003-6935

Mueller, G.; Amin, R.S.; Guagliardo, D.; McFeron, D.; Lundock, R.; Reitze, D.H. & Tanner, D.B. (2002). Method for compensation of thermally induced modal distortions in the input optical components of gravitational wave interferometers. *Classical and Quantum Gravity*, Vol.19, (1793-1801), 0264-9381

Mukhin, I.B. & Khazanov, E.A. (2004). Use of thin discs in Faraday isolators for high-average-power lasers. *Quantum Electronics*, Vol.34, No.10, (973-978), 1063-7818

Mukhin, I.B.; Voitovich, A.V.; Palashov, O.V. & Khazanov, E.A. (2009). 2.1 tesla permanent - magnet Faraday isolator for subkilowatt average power lasers. *Optics Communications*, Vol.282, (1969-1972), 0030-4018

Nicklaus, K.; Daniels, M.; Hohn, R. & Hoffmann, D. (2006). Optical isolator for unpolarized laser radiation at multi-kilowatt average power. *Proceedings of Advanced Solid-State Photonics,* pp. MB7, Incline Village, Nevada, USA

Palashov, O.V.; Voitovich, A.V.; Mukhin, I.B. & Khazanov, E.A. (2009). Faraday isolator with 2.5 tesla magnet field for high power lasers. *Proceedings of CLEO /EUROPE-EQEC 2009,* pp. CA1.6 MON, Munich, Germany

Poteomkin, A.K. & Khazanov, E.A. (2005). Calculation of the laser-beam M2 factor by the method of moments. *Quantum Electronics*, Vol.35, No.11, (1042-1044), 1063-7818

Raja, M.Y.A.; Allen, D. & Sisk, W. (1995). Room-temperature inverse Faraday effect in terbium gallium garnet. *Applied Physics Letters*, Vol.67, No.15, (2123-2125), 0003-6951

Ripin, D.J.; Ochoa, J.R.; Aggarwal, R.L. & Fan, T.Y. (2004). 165-W cryogenically cooled Yb:YAG laser. *Optics Letters*, Vol.29, No.18, (2154-2156), 0146-9592

Robinson, C.C. (1964). The Faraday rotation of diamagnetic glasses from 0.334 micrometer to 1.9 micrometer. *Applied Optics*, Vol.3, No.10, (1163-1166), 0003-6935

Roth, M.S.; Wyss, E.W.; Graf, T. & Weber, H.P. (2004). End-pumped Nd:YAG laser with self-adaptive compensation of the thermal lens. *IEEE Journal of Quantum Electronics*, Vol.40, No.12, (1700-1703), 0018-9197

Rubinstein, C.B.; Uitert, L.G.V. & Grodkiewicz, W.H. (1964). Magneto-optical properties of rare earth (III) aluminum garnets. *Journal of Applied Physics,* Vol.35, No.10, (3069-3070), 0021-8979

Scott, W.C. & de Wit, M. (1971). Birefringence compensation and TEM_{00} mode enhancement in a Nd:YAG laser. *Applied Physics Letters*, Vol.18, No.1, (3-4), 0003-6951

Shiraishi, K.; Tajima, F. & Kawakami, S. (1986). Compact Faraday rotator for an optical isolator using magnets arranged with alternating polarities. *Optics Letters*, Vol.11, No.2, (82-84), 0146-9592

Slack, G.A. & Oliver, D.W. (1971). Thermal conductivity of garnets and phonon scattering by rare-earth ions. *Physical Review B*, Vol.4, No.2, (592-609), 1098-0121

Soms, L.N. & Tarasov, A.A. (1979). Thermal deformation in color-center laser active elements. 1.Theory. *Soviet Journal of Quantum Electronics*, Vol.9, No.12, (1506-1508), 0049-1748

Tabor, M.J. & Chen, F.S. (1969). Electromagnetic propagation through materials possessing both Faraday rotation and birefringence: experiments with ytterbium orthoferrite. *Journal of Applied Physics*, Vol.40, No.7, (2760-2765), 0021-8979

VIRGO-Collaboration. (2008). In-vacuum optical isolation changes by heating in a Faraday isolator. *Applied Optics*, Vol.47, No.31, (5853-5861), 0003-6935

Voytovich, A.V.; Katin, E.V.; Mukhin, I.B.; Palashov, O.V. & Khazanov, E.A. (2007). Wide-aperture Faraday isolator for kilowatt average radiation powers. *Quantum Electronics*, Vol.37, No.5, (471-474), 1063-7818

Wynands, R.; Diedrich, F.; Meschede, D. & Telle, H.R. (1992). A compact tunable 60-dB Faraday optical isolator for the near infrared. *Review of Scientific Instruments*, Vol.63, No.12, (5586-5590), 0034-6748

Yasuhara, R.; Yamanaka, M.; Norimatsu, T.; Izawa, Y.; Kawashima, T.; Ikegawa, T.; Matsumoto, O.; Sekine, T.; Kurita, T.; Kan, H. & Furukawa, H. (2005). Design and analysis on face-cooled disk Faraday rotator under high average power lasers. *Proceedings of Advanced Solid-State Photonics*. pp. MB43, Vienna, Austria

Yasuhara, R.; Tokita, S.; Kawanaka, J.; Kawashima, T.; Kan, H.; Yagi, H.; Nozawa, H.; Yanagitani, T.; Fujimoto, Y.; Yoshida, H. & Nakatsuka, M. (2007). Cryogenic temperature characteristics of Verdet constant on terbium gallium garnet ceramics. *Optics Express*, Vol.15, No.18, (11255-11261), 1094-4087

Yoshikawa, A.; Kagamitani, Y.; Pawlak, D.A.; Sato, H.; Machidab, H. & Fukudaa, T. (2002). Czochralski growth of $Tb_3Sc_2Al_3O_{12}$ single crystal for Faraday rotator *Materials Research Bulletin,* Vol.37, No.1, (1-10), 0025-5408

Zarubina, T.V.; Kim, T.A.; Petrovskiy, G.T.; Smirnova, L.A. & Edel'man, I.S. (1987). Temperature dependence and dispersion of Faraday effect in glass based on oxide of terbium and cerium. *Optiko-mechanicheskaya Promyshlennost'*, Vol.11, (33-45), 1070-9762

Zarubina, T.V. & Petrovsky, G.T. (1992). Magnetooptical glasses made in Russia. *Opticheskii Zhurnal*, Vol.59, No.11, (48-52), 1070-9762

Zarubina, T.V.; Mal'shakov, A.N.; Pasmanik, G.A. & Poteomkin, A.K. (1997). Comparative characteristics of magnetooptical glasses. *Opticheskii Zhurnal*, Vol.64, No.11, (67-71), 1070-9762

Zarubina, T.V. (2000). Private communication.

Zelenogorsky, V.; Palashov, O. & Khazanov, E. (2007). Adaptive compensation of thermally induced phase aberrations in Faraday isolators by means of a DKDP crystal. *Optics Communications*, Vol.278, No.1, (8-13), 0030-4018

Zheleznov, D.S.; Voitovich, A.V.; Mukhin, I.B.; Palashov, O.V. & Khazanov, E.A. (2006). Considerable reduction of thermooptical distortions in Faraday isolators cooled to 77 K. *Quantum Electronics*, Vol.36, No.4, (383-388), 1063-7818

Zheleznov, D.S.; Khazanov, E.A.; Mukhin, I.B.; Palashov, O.V. & Voytovich, A.V. (2007). Faraday rotators with short magneto-optical elements for 50-kW laser power. *IEEE Journal of Quantum Electronics*, Vol.43, No.6, (451-457), 0018-9197

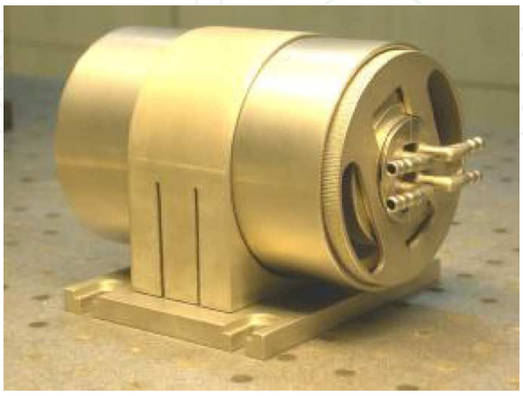

Faraday isolator with slab magnetooptical elements

Faraday isolator with strong magnet field

Faraday isolator for vacuum application

Advances in Solid State Lasers Development and Applications

Edited by Mikhail Grishin

ISBN 978-953-7619-80-0
Hard cover, 630 pages
Publisher InTech
Published online 01, February, 2010
Published in print edition February, 2010

Invention of the solid-state laser has initiated the beginning of the laser era. Performance of solid-state lasers improved amazingly during five decades. Nowadays, solid-state lasers remain one of the most rapidly developing branches of laser science and become an increasingly important tool for modern technology. This book represents a selection of chapters exhibiting various investigation directions in the field of solid-state lasers and the cutting edge of related applications. The materials are contributed by leading researchers and each chapter represents a comprehensive study reflecting advances in modern laser physics. Considered topics are intended to meet the needs of both specialists in laser system design and those who use laser techniques in fundamental science and applied research. This book is the result of efforts of experts from different countries. I would like to acknowledge the authors for their contribution to the book. I also wish to acknowledge Vedran Kordic for indispensable technical assistance in the book preparation and publishing.

How to reference

In order to correctly reference this scholarly work, feel free to copy and paste the following:

Efim Khazanov (2010). Faraday Isolators for High Average Power Lasers, Advances in Solid State Lasers Development and Applications, Mikhail Grishin (Ed.), ISBN: 978-953-7619-80-0, InTech, Available from: http://www.intechopen.com/books/advances-in-solid-state-lasers-development-and-applications/faraday-isolators-for-high-average-power-lasers

INTECH
open science | open minds

InTech Europe
University Campus STeP Ri
Slavka Krautzeka 83/A
51000 Rijeka, Croatia
Phone: +385 (51) 770 447
Fax: +385 (51) 686 166
www.intechopen.com

InTech China
Unit 405, Office Block, Hotel Equatorial Shanghai
No.65, Yan An Road (West), Shanghai, 200040, China
中国上海市延安西路65号上海国际贵都大饭店办公楼405单元
Phone: +86-21-62489820
Fax: +86-21-62489821

IntechOpen